

# The deep background of large-scale, Mesozoic Cu-Au-W metallogenesis in northeastern South China: Constraints from Yingshan-Changshan wide-angle seismic reflection/refraction data

Jue HOU<sup>1,3,4</sup>, Tao XU<sup>1,5\*</sup>, Qingtian LÜ<sup>2</sup>, Zhiming BAI<sup>1,5</sup>, Yongqian ZHANG<sup>2</sup>, Zhiyu ZHANG<sup>6</sup> & Dan YANG<sup>7</sup>

<sup>1</sup> State Key Laboratory of Lithospheric Evolution, Institute of Geology and Geophysics, Chinese Academy of Sciences, Beijing 100029, China;

<sup>2</sup> China Academy of Geological Sciences, Beijing 100037, China;

<sup>3</sup> Institute of Geophysics, China Earthquake Administration, Beijing 100081, China;

<sup>4</sup> University of Chinese Academy of Sciences, Beijing 100049, China;

<sup>5</sup> Innovation Academy for Earth Science, Chinese Academy of Sciences, Beijing 100029, China;

<sup>6</sup> Institute of Geology, China Academy of Geological Sciences, Beijing 100037, China;

<sup>7</sup> Institute of Mineral Resources, China Academy of Geological Sciences, Beijing 100037, China

Received February 19, 2022; revised June 14, 2022; accepted June 20, 2022; published online September 20, 2022

**Abstract** To investigate the geodynamic processes of Mesozoic large-scale mineralization in South China, we deployed a 350-km-long, wide-angle seismic reflection/refraction sounding profile between Yingshan in Hubei and Changshan in Zhejiang. This profile traverses the Cu-Au metallogenic belt in the middle and lower reaches of the Yangtze River (YMB), the Jiangnan W-polymetal metallogenic belt (JNMB), and the Qinhang Cu-polymetal metallogenic belt (QHMB). Our imaging results reveal various interesting velocity features along the profile. (1) The velocity structure is characterized by vertical layering and horizontal blocking; (2) the YMB is marked by high velocity and high  $V_p/V_s$  ratios in general with a significantly uplifted Moho interface and a thin crust of ~31 km, and the lower crust contains high-velocity anomalies and has the characteristics of a crust-mantle transition zone; (3) the JNMB is bounded by the Jiangnan fault and Jingdezhen-Huangshan fault and has low-velocity anomalies and low  $V_p/V_s$  ratios; and (4) the QHMB is characterized by high-velocity anomalies and high  $V_p/V_s$  ratios. The high-velocity anomalies in the YMB and QHMB represent relatively Cu-Au-rich mafic juvenile lower crust. The formation of this kind of crust is considered to be related to mantle-derived magma underplating or residues of Neoproterozoic oceanic crustal materials, and it also provided sources for large-scale Cu-Au mineralization in the Mesozoic. The JNMB has features similar to those of ancient crusts enriched in W-Sn, the partial melting of which played a leading role in the formation of the superlarge W deposits in this belt. Considering these results and other regional geological data, we propose that a large-scale oblique upwelling of the asthenosphere along the collisional belt of the Yangtze and Cathaysia blocks during the Mesozoic was the deep driving mechanism for the explosive mineralization of Cu, Au, and W in northeastern South China. The boundaries of the blocks or terrains and discontinuities of the lithosphere were the main channels for deep heat and magmas and therefore controlled the spatial distribution of the metallogenic belt.

**Keywords** Northeastern South China, Metallogenic belt of the middle and lower reaches of the Yangtze River, Wide-angle seismic reflection/refraction, Yingshan-Changshan seismic profile, Crustal velocity structure.

**Citation:** Hou J, Xu T, Lü Q, Bai Z, Zhang Y, Zhang Z, Yang D. 2022. The deep background of large-scale, Mesozoic Cu-Au-W metallogenesis in northeastern South China: Constraints from Yingshan-Changshan wide-angle seismic reflection/refraction data. *Science China Earth Sciences*, 65(11): 2202–2218, <https://doi.org/10.1007/s11430-022-9973-4>

\* Corresponding author (email: [xutao@mail.iggcas.ac.cn](mailto:xutao@mail.iggcas.ac.cn))

## 1. Introduction

South China experienced large-scale deformation, extensive volcanic eruptions, and polymetallic mineralization in the Mesozoic (Wang, 2009). In recent decades, many studies focusing on deformation mechanisms, magmatism and metallogenic mechanisms have been carried out in South China, with multiple models proposed, such as the continent-continent collision model (Hsü et al., 1988, 1990), paleo-oceanic plate subduction model (Zhou and Li, 2000; Wang et al., 2011; Li et al., 2006; Li and Li, 2007; Sun et al., 2007), multiplate interaction model (Dong et al., 2007; Wang, 2009), intraplate tension/rift model (Wang Y J et al., 2013; He et al., 2007), mantle plume model (Xie et al., 1997; Zhang et al., 2009), and strike-slip model (Xu et al., 1987; Gilder et al., 1996). Liu et al. (2013) summarized these viewpoints and pointed out that the incongruity of these models, on the one hand, reflects the complexity of the geological evolution of South China since the Proterozoic and, on the other hand, indicates the lack of geophysical observations on the deep structure.

The northeastern part of South China is not only the epitome of the tectonic evolution of all of South China but also the key area to study the intracontinental orogeny and associated large-scale mineralization. There are three worldclass Mesozoic metallogenic belts (Figure 1), namely the metallogenic belt of the middle and lower reaches of the Yangtze River (YMB), the Jiangnan metallogenic belt (JNMB), and the Qinhang metallogenic belt (QHMB), respectively. The YMB is located on the northern margin of the Yangtze block and has a “V”-shape that is narrow in the southwest and wide in the northeast (Chang et al., 1991; Lü et al., 2005, 2014; Zhang et al., 2014). This belt includes seven large ore-concentrated areas and more than 200 large and medium-sized ore deposits (Figure 1) (Chang et al., 1991; Pan and Dong, 1999). Within this belt, the faulted-uplifted areas (e.g., Jurui, Anqing-Guichi, Tongling, and southeastern Hubei) are dominated by porphyry-skarn Cu-Au deposits, and the diagenesis and mineralization occurred 146–135 Ma, with a peak ~140 Ma (Chang et al., 1991; Zhai et al., 1992; Chen et al., 2001; Sun et al., 2003; Mao et al., 2006; Zhou et al., 2008a), whereas within the faulted-depression areas (e.g., Ningwu and Luzong), the mineralization is dominated by mafic porphyry iron ore deposits and occurred ~130 Ma. In addition, a younger gold-uranium metallogenic event was recently discovered to take place at 126–123 Ma, which was related to A-type granites (Zhou et al., 2008b, 2017). The JNMB is a newly delineated world-class W-Cu metallogenic belt (Figure 1) with a proven resource of 6.06 million tons (Mao et al., 2020). Located in the middle of the Yangtze block, the JNMB is spatially parallel to the YMB on the northern side and has a similar metallogenic time periods (150–135 and 130–125 Ma) to those of the YMB. The de-

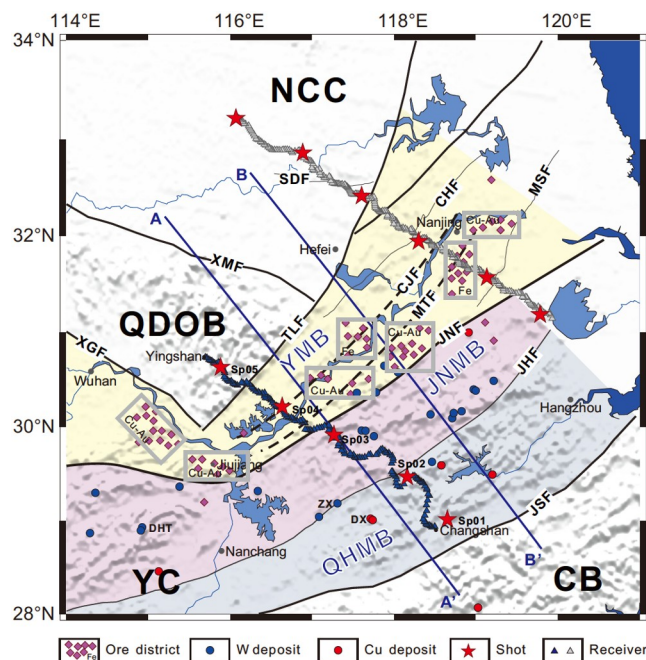


**Figure 1** The observation system of our wide-angle, reflection/refraction seismic profile in the middle section of the YMB. The red stars indicate shot points. The blue triangles indicate receivers. The gray triangles indicate the receivers along the Lixing-Yixing profile. The purple diamonds indicate the middle and lower reaches of the Yangtze metallogenic belt. NCC, North China Craton; QDOB, Qinling-Dabie orogenic belt; YC, Yangtze Craton; CB, Cathaysia Block; YMB, the metallogenic belt of the middle and lower reaches of the Yangtze River; JNMB, Jiangnan metallogenic belt; QHMB, Qinhang metallogenic belt; ZX, Zhuxi tungsten mine; DHT, Dahutang deposit; DX, Dexing copper mine; TLF, Tanlu fault; JHF, Jingdezhen-Huangshan fault; SDF, Shouxian-Dingyuan fault; CHF, Chuhe fault; MSF, Maoshan east lateral fault; JNF, Jiangnan fault; JSF, Jiangshao fault; CJF, Yangtze River fault; MTF, main thrust fault; XMF, Xiaotian-Mozitan fault; and XGF, Xiangfan-Guangji fault. Blue solid lines, AA' and BB', denote broadband flow seismic sections (Li et al., 2020) (the results are shown in Figure 10).

posits are mainly skarn-type, porphyry-like-type, and quartz vein-type, with representatives of the largest Zhuxi W deposits in the world (Chen et al., 2016; Ouyang et al., 2019), the superlarge Dahutang W-Cu deposit, which is rich in polymetallic mineralization (Xiang et al., 2012; Duan and Jiang, 2017), and the large-scale Dongping W deposit (Mao et al., 2020). The QHMB is located to the south of the JNMB and extends along the Neoproterozoic suture zone between the Yangtze and Cathaysia Blocks (Figure 1). It extends in a NE-SW direction from Hangzhou Bay in Zhejiang in the northeast to central Jiangxi and eastern Hunan Provinces and farther to Qinzhou Bay in Guangxi in the southwest and is ca. 2000 km long and 100–150 km wide (Yang and Mei, 1997). Large-scale deposits are widely distributed in the northeastern segment of the belt, in which mineralization was mainly copper and gold and the metallogenic age was approximately 175–160 Ma (Ni and Wang, 2017). Typical deposits include the Dexing superlarge porphyry Cu deposit, whose molybdenite Re-Os age was ca. 171 Ma (Wang et al.,

2015), the Yinshan Cu-Au polymetallic deposit (ca. 170 Ma) (Wang G G et al., 2013), and the Jiande Cu deposit (ca. 161 Ma) (Chen et al., 2017) (Figure 1).

Although numerous studies on the geological background and genetic mechanisms of large-scale Cu-Au-W-Sn mineralization in South China have been conducted, there are still three questions that need to be further addressed, including (1) why three generally parallel giant metallogenic belts developed intensively in the Mesozoic, in which the ore deposits and the metal clusters are located within a relatively long and narrow tectonic belt (Figure 1)? (2) Why Mesozoic explosive mineralization displays regional migration from south to north over time (170 to 125 Ma)? (3) Why are the two metallogenic belts in the north and south dominated by Cu-Au mineralization, but the central belt is dominated by W mineralization?

Recent studies, especially those of deep reflection seismology, have greatly increased the knowledge of the crustal and upper mantle structures in South China, promoting the understanding of the geology and formation mechanisms of large-scale Cu-Au-W-Sn mineralization (Dong et al., 1998, 2010; Zhang et al., 2011b; Lü et al., 2004, 2005, 2011, 2013, 2014, 2015; Liu et al., 2003; Hou et al., 2004; Dong et al., 2004; Jiang et al., 2013, 2014; Shi et al., 2013; Xu et al., 2014b; Gu et al., 2020; Zhang Y Q et al., 2021). However, due to the limitation of the data, it is still difficult to characterize the deep processes and driving mechanisms of the large-scale Mesozoic mineralization.

To better understand the deep structure and geodynamic evolution of tectonism-magmatism-mineralization in Southeast China, we deployed an active source wide-angle, reflection/refraction detection profile oriented in an NW direction that crosses the aforementioned three metallogenic belts (Figure 1). The profile lies between Changshan County in Zhejiang Province and Yingshan County in Hubei Province, passing through Hubei, Anhui, Jiangxi and Zhejiang Provinces, with the main part located within Anhui and Jiangxi Provinces (Xu et al., 2014b). Based on seismic data from this profile, we aim to reveal the fine-velocity structure of the crust and upper mantle and the relations between the geodynamics and velocity structure.

## 2. Tectonic setting

Figure 1 shows a brief structural framework of the study area. The study area is separated into four units by the Tan-Lu fault (TLF), Jiangnan fault (JNF), and Jingdezhen-Huangshan fault (JHF). They act as important boundary faults, dividing the study area into four major tectonic units (Figure 1).

The TLF is an NNE-oriented giant shear zone with a length of 2400 km, crossing the Qinling-Dabie collision orogen

(Gilder et al., 1999; Zhu et al., 2004a, 2004b; Zhu et al., 2005). The southern segment of the TLF displaces the Dabie orogenic belt and Sulu orogenic belt by 550 km in a sinistral movement sense (Zhu et al., 2004a; Chang et al., 2012).

The YMB is bounded by the JNF to the southeast and the TLF to the northwest (Figure 1). A peculiar characteristic of the YMB is “one cap and multiple bases” (Chang et al., 1991, 1996), meaning that it has multiple continental crust basements and a unified stratigraphic cap. Influenced by the Indonesian movement, the YMB was strongly folded and received continental basin deposits in the Middle Jurassic. Yanshanian (145–120 Ma) tectonic-magmatic activities developed mainly along the Yangtze River and were concentrated in seven ore concentration areas (Lü et al., 2007, 2014; Xu et al., 2014b). Among these, the Tongling ore concentration area is characterized by high-potassium calc-alkaline rock assemblages, the Ningwu and Luzong areas by high-sodium calc-alkaline intrusive rocks and shoshonite-series volcanic assemblages, and the southeastern Hubei uplift-depression transition area by calc-alkaline-alkaline igneous rocks (Chang et al., 1991; Xing and Xu, 1999; Zhou et al., 2008b). The mineralization within the YMB is mainly related to Yanshanian adakitic intrusive rocks (Wang Y et al., 2004; Song et al., 2011).

The Jiang-Shao fault (JSF) and Jiangnan fault (JNF) are the southern and northern boundaries of the JNMB, respectively, and the YMB lies to its north and the QHMB to its south. The basement of the JNMB is considered to be composed of Mesoproterozoic Tianli schist, lower Neoproterozoic Shuangxiwu pyroclastic rocks, and mid-Neoproterozoic phyllites and metavolcanic sedimentary rocks of the Shuangxiwu Group (~830 Ma). The overlying strata distributed around the paleo-Jiangnan continent comprise Lower Jurassic marine facies and marine-terrestrial interfacies clastic and carbonate rocks, and Middle-Lower Jurassic volcanic-sedimentary rock. In addition, the Neoproterozoic Jiuling granite-diorite batholith (828±8 Ma), the largest granitic batholith in South China (Wang X L et al., 2017; Duan et al., 2019), is intruded by small Mesozoic granitic plutons (152–125 Ma). It is these granitic plutons are accompanied by large-scale W mineralization forming the world-class W metallogenic province (Feng et al., 2012; Huang and Jiang, 2013; Chen et al., 2016; Mao et al., 2020).

The JSF is the boundary between the Yangtze and Cathaysia blocks. The Jiangnan orogenic belt to the north is a Meso-Neoproterozoic orogenic belt developed along the southern margin of the Yangtze block (Zheng et al., 2008; Wang Y J et al., 2013; Zhao, 2015). There are small amounts of dismembered ophiolite fragments (1.1–0.83 Ga) (Li et al., 1997, 2009; Yao et al., 2016) and island arc basalts (0.89–0.97 Ga), recording the subduction of the paleo-oceanic basin and the continent-continent collision between the Yangtze and Cathaysian blocks. Because of the intense

Triassic collisional orogenesis around, this orogenic belt experienced strong compression and uplift. It was then affected in the Middle Jurassic by magmatism in an extensional setting, leading to the formation of many small stocks and plutons represented by the Dexing porphyry.

### 3. Yingshan-Changshan profile wide-angle seismic reflection/refraction data

#### 3.1 Seismic data acquisition

Figure 1 shows the 350-km-long profile extending between Yingshan and Changshan. It crosses the main tectonic units from southeast to northwest. From November 2013 to January 2014, five active blasts at separated sites (a total of 9.9 tons of TNT equivalent) were triggered along the detection profile, and seismic wave fields were excited by combined blasting downholes. The distances between the five blasting points ranged from 60 to 100 km. 160 PDS-2 portable three-component digital seismographs were deployed in the profile for recording seismic waves. The observation system can record seismic waves propagating from different depths and infer properties of the crust and upper mantle, mapping the crustal structure of northeastern South China.

#### 3.2 Seismic phase analysis and data processing

Seismic phase recognition includes recognizing the seismic phases of reflection and refraction from the crystalline substrate of the shallow crust, which manifests as the first arrivals on all record sections. The Pm phases are reflection phases from the first-order discontinuous Moho surface; and the Pn phases are the refracted waves of the weak velocity gradient layer at the top of the upper mantle with an apparent velocity of 8.0–8.1 km s<sup>-1</sup>. The reflected waves of the secondary velocity discontinuities in the crust have relatively weak energy, and therefore, these reflected waves at different regions are grouped into different groups, collectively referred to as the Pc phase, with different groups named the P1, P2 and P3 phases. We obtained crust and upper mantle structures after several rounds of revising the model and calculating the fitting of the multiple seismic phases of the travel time by ray tracing forward calculation (Cerveny et al., 1988; Vidale, 1988; Zelt and Smith, 1992; Cerveny, 2001; Xu et al., 2004, 2006a, 2010, 2014a). In the procedure of seismic phase fitting, the intercept of the seismic phase curve mainly reflects the depth of the reflection interface, and the slope of the seismic phase curve mainly reflects the average velocity of the strata above the interface, such as the Pm phase. The apparent velocity at the far offset is approximately the velocity of the lower crust of the reflection point (Figures 2–6).

#### 3.3 Traveltime fitting and ray coverage

The traveltime fitting results (Figure 7) and ray coverage map (Figure 8) of the five shots show that the ray coverage density of the section in this area is sufficient, the traveltime fitting is very ideal, and the two-dimensional velocity obtained by the traveltime fitting is reliable.

#### 4. Velocity structure of the Yingshan-Changshan profile

As shown in Figure 9, the profile has a 3-layered crustal structure, including the upper (the bottom interface is buried at a depth of approximately 12 km), middle (the bottom interface is buried at a depth of approximately 26 km), and lower crust (the bottom interface is buried at a depth of approximately 31–35 km).

(1) The P-wave velocity at the top interface of the crystalline basement of the upper crust is approximately 5.8 km s<sup>-1</sup>, the depth is approximately 2 km, and the horizontal direction shows obvious fluctuation characteristics. In the Dabie orogenic belt, the upper crust exhibits obvious high-velocity characteristics, and the shallow surface reaches approximately 6.0 km s<sup>-1</sup>, which corresponds well with the Triassic ultrahigh-pressure metamorphic belt exposed on the surface. In the lower Yangtze region and the northern part of the Jiangnan uplift belt, affected by factors such as sedimentary depressions and the Yangtze River Basin, the upper crust exhibits low-velocity anomalies (horizontal stakes 125–260 km).

(2) The mid-crust depth of the profile is approximately 12–26 km, and the velocity is 6.2–6.5 km s<sup>-1</sup>, which is slightly lower in the lower Yangtze region; the lateral inhomogeneity is not very obvious, and the results are also related to the resolution of the data.

(3) The lower crust velocity is laterally inhomogeneous. The lateral change in the Moho interface depth is within a range of 33–35 km and with a weak uplift below the YMB (the horizontal pile number is approximately 125 km). The undulation of the Moho interface is consistent with a high Bouguer gravity anomaly (Figure 9a). Furthermore, the velocity structure shows obvious horizontal blocking characteristics, taking the JNF and JHF as boundaries. West of the JNF, the velocity of the lower crust is as high as 6.7–6.9 km s<sup>-1</sup> beneath the Qinling-Dabie orogeny and YMB (horizontal stake 50–150 km). To the east of the JHF, the lower crustal velocity is 6.6–6.8 km s<sup>-1</sup>, showing high-velocity anomalies beneath the Jiangnan orogenic belt (section horizontal stake number 260–300 km). Between the JNF and JHF, the lower crustal velocity is 6.5–6.6 km s<sup>-1</sup>, showing a relatively low-velocity anomaly beneath the JNMB (the horizontal pile number of the profile is 150–260 km).

The Moho depth (33–35 km) of the Yingshan-Changshan

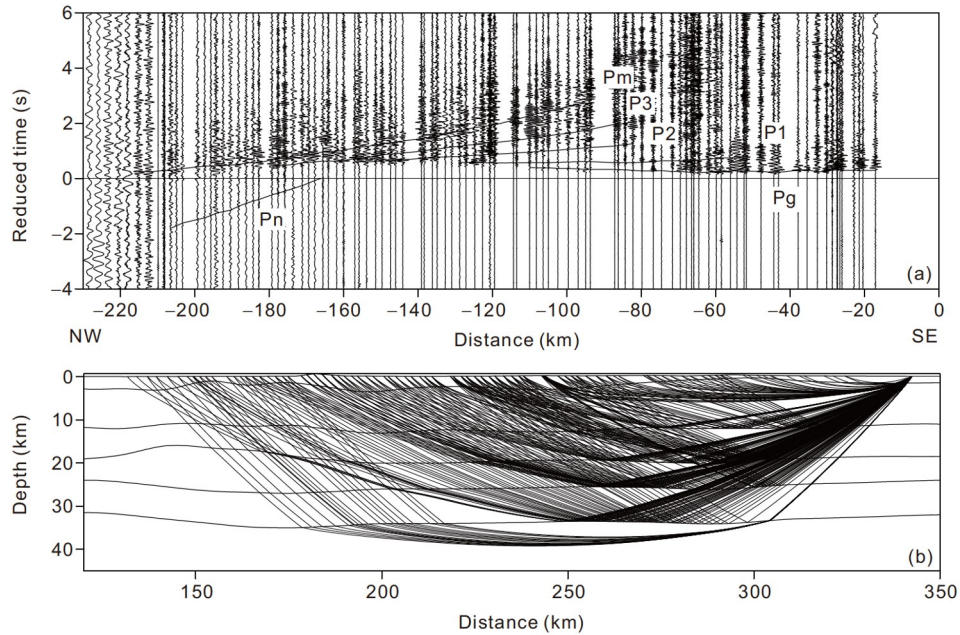


**Figure 2** Shot point Sp01 of the Yingshan-Changshan profile. (a) Seismic phase picking and travel time fitting; (b) ray tracing results.

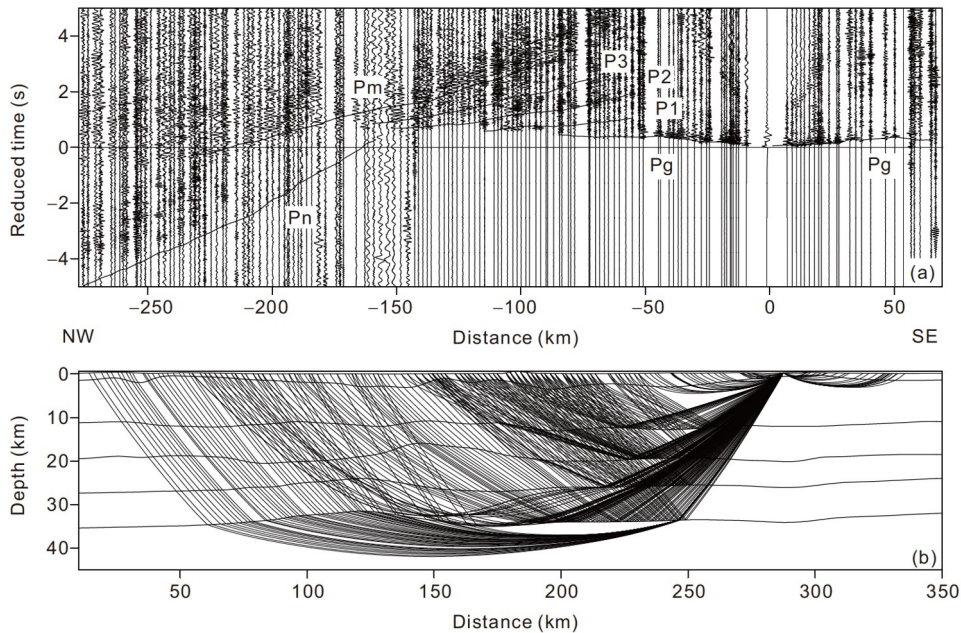


**Figure 3** Shot point Sp02 of the Yingshan-Changshan profile. (a) Seismic phase picking and travel time fitting; (b) ray tracing results.

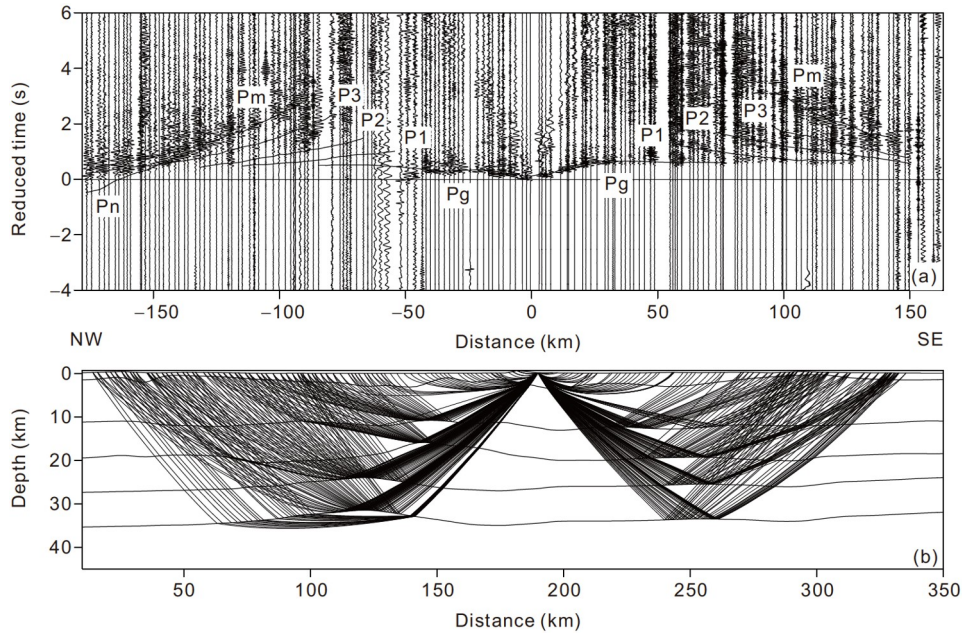
profile is consistent with previous results (Wang et al., 2000; Bai and Wang, 2006; Xu et al., 2014b; Zheng et al., 2014; Zhang et al., 2015).

Figure 10 shows the crustal S-wave velocity of the middle and lower reaches of the YMB and its adjacent areas obtained by ambient noise tomography using the data of the NCISP-8 array (Li et al., 2020). Overall, the lower crustal velocity from this study is relatively consistent with those from ambient noise tomography. As shown in Figure 10a, in the JNMB, the lower crust displays a low-velocity anomaly,

while in the YMB (north of the JNF) and QHMB (between the JHF and JSF), the lower crust displays an obvious high-velocity anomaly. The range of the low-velocity area of the profile in Figure 10b is slightly different, perhaps caused by the far distance between the BB' profile and our profile.

## 5. Discussion

The deep crust and upper mantle structure contain key in-



**Figure 4** Shot point Sp03 of the Yingshan-Changshan profile. (a) Seismic phase picking and travel time fitting; (b) ray tracing results.

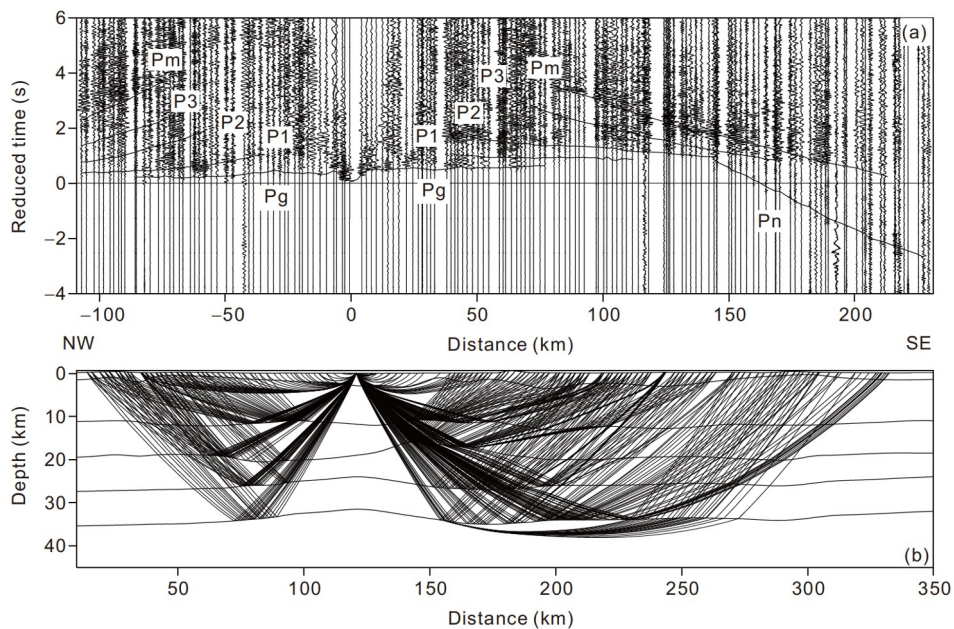


**Figure 5** Shot point Sp04 of the Yingshan-Changshan profile. (a) Seismic phase picking and travel time fitting; (b) ray tracing results.

formation related to the metallogenic background and metallogenic processes (Hou et al., 2007; Richards, 2011; Luo et al, 2012; Ouyang et al., 2014; Lü et al., 2015a, 2021; Wang et al., 2021). Therefore, analyzing the deep structures can provide key constraints for the construction of the spatial model of the metallogenic system (source-transport-reservoir) and for the migration and mineralization processes of ore-forming fluids.

The structural and physical parameters, such as the

thickness, velocity, and  $V_p/V_s$  of the crust, are closely related to the formation and evolution of the continental crust (Xu et al., 2006b). Provided a tectonic compression environment under the same temperature and pressure conditions, felsic rocks are more likely to form nappe structures or tight folds than mafic rocks, resulting in a decrease in  $V_p/V_s$  with increasing crustal thickness (Wang, 2007). In addition, delamination reduces the thickness of the mafic rocks in the lower crust and can also reduce the Poisson's ratio of the

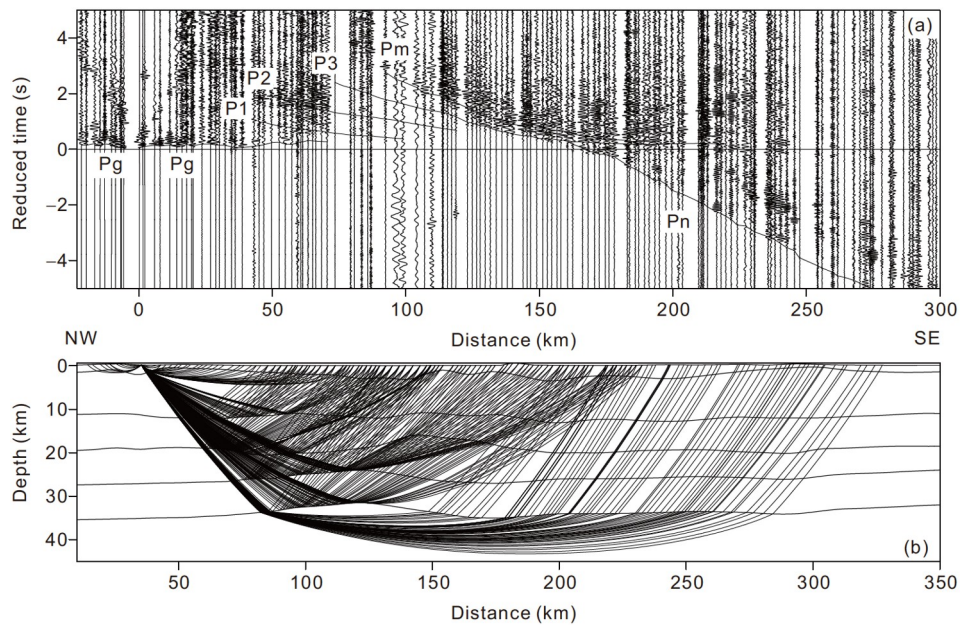


**Figure 6** Shot point Sp05 of the Yingshan-Changshan profile. (a) Seismic phase picking and travel time fitting; (b) ray tracing results.

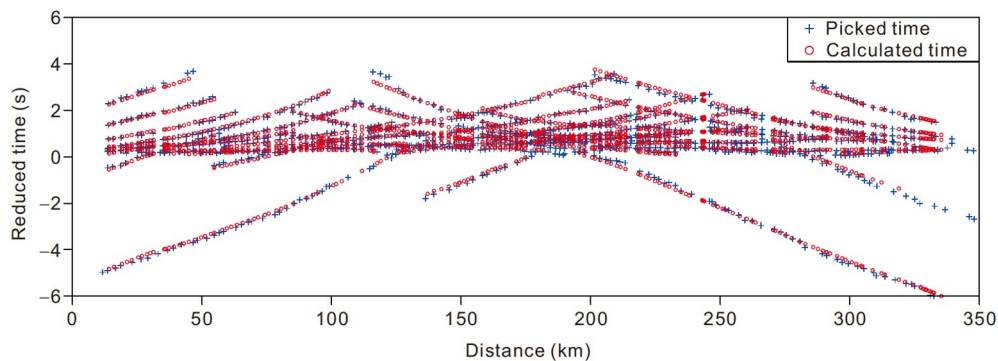


**Figure 7** Traveltime fitting results of the five shots in the Yingshan-Changshan profile. Blue crosses denote picked traveltimes, and red circles denote calculated times.

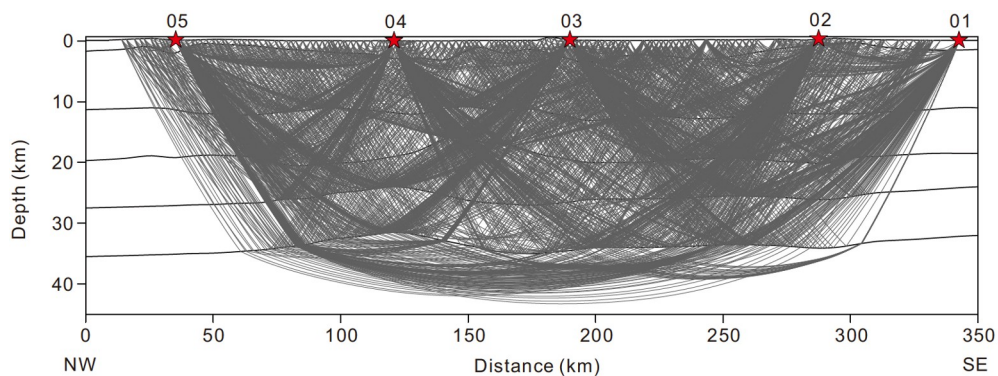


**Figure 8** Seismic ray coverage of five shots in the Yingshan-Changshan profile.

crust (Zandt and Ammon, 1995; Gao et al., 1998). When the mafic magma migrates upward from the upper mantle to the crust-mantle interface, magma underplating often occurs,

and the magma is further emplaced in the crust, which increases the Poisson's ratio of the crust (Ji et al., 2009).

Magma is the "probe" of deep processes. Nd-Hf-isotope

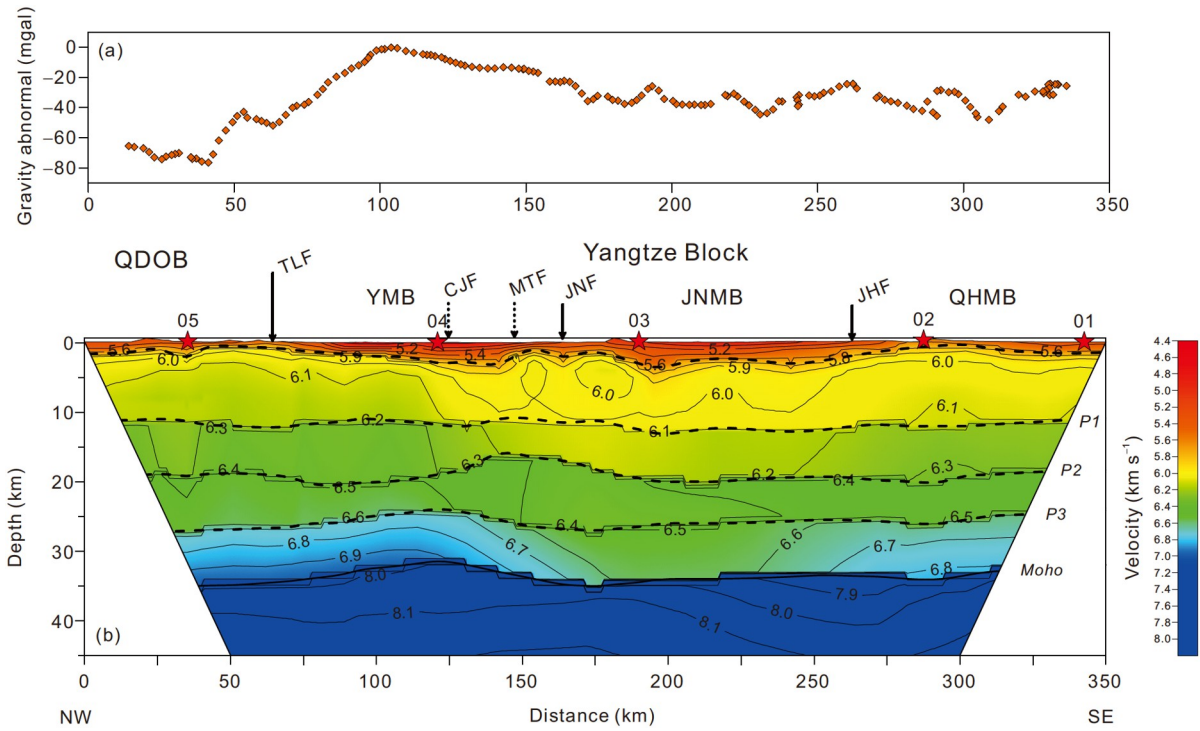


**Figure 9** Satellite Bouguer gravity anomaly curve (a) and two-dimensional crustal velocity structure (b) in the Yingshan-Changshan profile. QDOB, Qinling-Dabie orogenic belt; YMB, the metallogenic belt of the middle and lower reaches of the Yangtze River; JNMB, Jiangnan metallogenic belt; QHMB, Qinhang metallogenic belt; TLF, Tanlu fault; JNF, Jiangnan fault; JHF, Jingdezhen-Huangshan fault; CJF, Yangtze River fault; and MTF, main thrust fault.

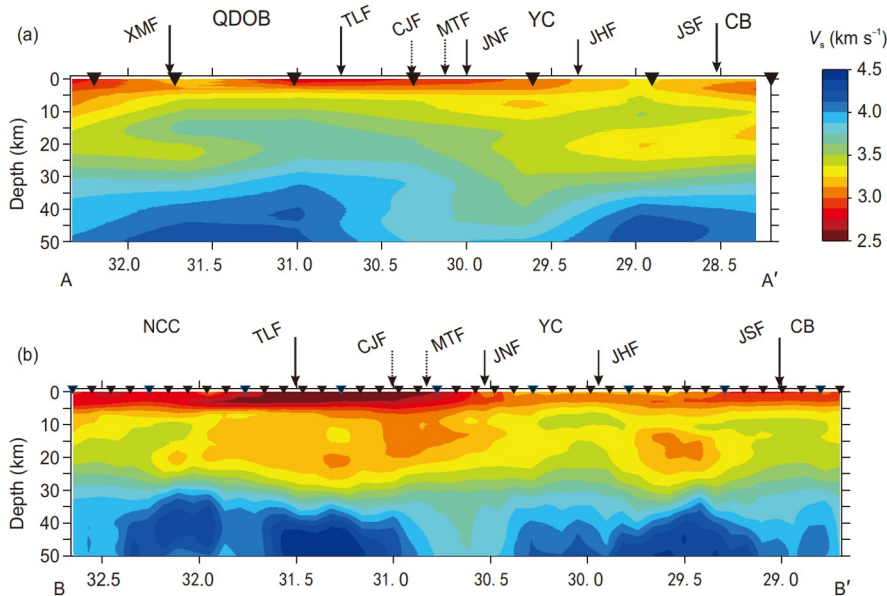


**Figure 10** Crustal S-wave velocity structure in the middle and lower reaches of the Yangtze River and its adjacent areas (modified from Li et al., 2020). AA', BB'; see Figure 1 for section locations; NCC, North China Craton; QDOB, Qinling-Dabie orogenic belt; YC, Yangtze Craton; CB, Cathaysia block; XMF, Xiaotian-Mozitan fault; TLF, Tanlu fault; JNF, Jiangnan fault; JHF, Jingdezhen-Huangshan fault; JSF, Jiangshao fault; CJF, Yangtze River fault; and MTF, main thrust fault.

mapping of magmatic rocks is an efficient geochemical means to uncover the properties, composition, and time evolution of magma source regions (Hou et al., 2015; Hou and Wang, 2018). Shallow mineral deposits are the product

of four-dimensional lithospheric evolution and deep material and energy exchange, and the metal mineralization assemblages can also record the source and cycling processes of metals during lithospheric evolution. Therefore, mutual

constraints between the analysis of regional magmatic and metallogenic assemblages and the observation of velocity structures and physical property parameters will make it highly possible to restore the deep crust-mantle structure, trace the deep processes, and reveal the geodynamic mechanisms based on the preserved geophysical-geochemical vestiges. Following this idea, we attempt to discuss the following three issues through multidisciplinary constraints.

### 5.1 Lateral structural variation of the Yangtze block and block differences

Our Yingshan-Changshan seismic profile and previous A-A' and B-B' profiles cross the whole northeastern Yangtze block and show the lateral structural changes of the Yangtze block, which is characterized by obvious zoning features (Figures 9 and 10). As mentioned above, the JNF and JHF divide the Yangtze block into three subblocks: the northern (margin), central (paleoland), and southern (margin) blocks, which correspond to the YMB, JNMB, and QHMB, respectively (Figure 1). These blocks have different geological evolutionary processes and thus show differences in velocity, composition, and crustal thickness.

#### 5.1.1 Velocity structural differences

This is particularly evident in the lower crustal velocity of the three blocks. The lower crust in the northern block, located to the north of the JNF fault, displays a distinct high-velocity anomaly, with velocities reaching up to  $6.7\text{--}6.9\text{ km s}^{-1}$  (Figure 9). The Yingshan-Changshan and A-A' profiles show that the high-velocity anomaly extends northward to the Dabie orogenic belt (Figures 9 and 10a), consistent with previous wide-angle seismic reflection/refraction imaging results (Wang et al., 2000). These profiles show that the South Dabie has a composition similar to that of the YMB, implying that the northern edge of the Yangtze block was underthrust beneath the Dabie orogen. The B-B' profile shows that the high-velocity anomaly extends to the northern side of the TLF and that it contrasts with the high-velocity anomaly of the lower crust of the North China block, indicating that part of the Yangtze block subducted beneath the North China block during the Triassic collision. The middle-upper crust of the northern block has a high velocity over a large area, consistent with the geological features of widespread Mesozoic magma emplacement and consolidation processes in the YMB. The lower crust of the southern block to the south of the JNF also has a high-velocity anomaly ( $\sim 6.6\text{--}6.8\text{ km s}^{-1}$ ) (Figure 9), especially the middle area between the JHF and JSF, which corresponds to the Jiangnan orogenic belt (Figure 10b). The high velocity may have been caused by early Mesoproterozoic accretion and Neoproterozoic collision on the southern edge of the Yangtze block (Wang et al., 2000). The velocity of the middle crust of

the southern block is somewhat lower than the velocity of the northern block. The velocity of the middle block is relatively low ( $6.5\text{--}6.6\text{ km s}^{-1}$ ) (Figure 9). The A-A' and B-B' profiles show that the area of the low-velocity anomaly of the lower crust decreases gradually from southwest to northeast (Figure 10). The average P-wave velocity of the crust in the middle block is  $6.4\text{ km s}^{-1}$ , consistent with that of cratons (Zhang et al., 2011a, 2011b). The low-velocity ( $V_p < 6.1\text{ km s}^{-1}$ ) features and scopes in the upper crust of the middle block are also consistent with the distribution of the pre-Sinian-Triassic vastly thick ( $>10\text{ km}$ ) marine turbidite flysch deposits and marine volcanic-sedimentary rock series developed on the metamorphic basement in this area (Chang et al., 1996; Dong et al., 2011) and with regional crustal shortening and thickening. Therefore, the velocity structure essentially reflects the crustal structural characteristics of the Yangtze Craton.

#### 5.1.2 Compositional structural differences

The  $V_p/V_s$  ratios can reflect the composition of the crust. The higher the  $V_p/V_s$  ratio is, the higher the proportion of mafic material in the crust. The higher proportion of mafic material indicates a greater amount of mantle-derived components added to the crust. Figure 11a shows the  $V_p/V_s$  ratio in the study area reconstructed on the basis of Zhang Y Q et al. (2021), which is consistent with the results obtained by receiver function and surface wave dispersion (Li et al., 2018). Figure 11a exhibits a positive correlation between the  $V_p/V_s$  ratio and the velocity structure of the lower crust. The results show that the northern block generally displays high  $V_p/V_s$  ratios ( $\geq 1.78$ ), and the high anomaly areas are concentrated in the Luzong, Anqing, Guichi, and other ore-concentrated areas, corresponding to the YMB. The area between the JHF and JSF also shows high  $V_p/V_s$  anomalies, and the high anomaly areas are those concentrated in Cu-Au mineralization, such as Dexing (Figure 11a). In contrast, the middle block has relatively low  $V_p/V_s$  ratios, and the low velocity anomaly area is located in the central-western part of the central block (Figure 11a), corresponding to the areas where the Zhuxi and Dahutang W deposits are situated. These results indicate that the lower crust of the northern and southern blocks, characterized by high-velocity anomalies, is mainly mafic in composition, indicating that it contains more mantle-derived components, while the central block featured by low-velocity anomalies is generally intermediate in composition (andesitic) and contains less mantle-derived materials. From the distribution characteristics of the  $V_p/V_s$  ratio, we conclude that the crustal composition of the Yangtze block is very uneven. In general, the eastern part of the three blocks is more mafic in composition, while the west is more intermediate. From the perspective of the distribution of the mineral deposits, the Cu-Au deposits are mainly located in mafic domains, whereas the W deposits are less

mafic (Figure 11a).

### 5.1.3 Differences in crustal thickness

The Moho depth obtained from our P-wave velocity structure shows obvious lateral differences. Figure 9 shows that the Moho depth is significantly shallower under the northern block, with the thinnest crust (~31 km) among the three blocks, is approximately horizontal and slightly thicker (~34 km) under the southern block, and is slightly concave (~35 km) beneath the central block. These results are generally similar to previous results. For example, Yan et al. (2011), using the Parker-Oldenburg method, obtained the Moho depth of the Yangtze block (Figure 11b) and found that the Moho surface is significantly higher (mantle ridge) in the YMB. The upper mantle ridge occurs generally along a line connecting Huaining-Zongyang-Chaohu, and the seven ore-concentrated areas developed mainly along the NE-trending mantle ridge or mantle slope (Figure 11b). Deep seismic reflection profiles show that the Moho depth in the Ningwu ore-concentrated area varies between 29 and 35 km (Lü et al., 2015b), with the deepest Moho areas beneath the Ningwu deposit (~29 km). Wide-angle, reflection/refraction seismic soundings show that the Moho depth in the Ningwu ore-concentrated area is approximately 32–33 km, and receiver function results show that the Moho depth in the metallogenic belt is approximately 28–36 km (Shi et al., 2013). The crustal thickness of the Jiangnan orogenic belt varies greatly. The Moho is deeper in the east than in the west. The Cu-Au mineralization areas, such as Dexing, are situated in the thinned crustal areas. The central block has the thickest crust (35 km) and hosts large and superlarge W deposits (Figure 11b). In short, the northern Yangtze block has the thinnest crust, with NE-trending mantle ridges; the southern block has a slightly thicker crust, and the Moho depth changes dramatically; and the central block is relatively stable and has the largest crustal thickness.

The inconsistency of the crustal thickness, velocity,  $V_p/V_s$  ratios, and other structural and physical parameters prove that the three blocks in the northern, southern and middle parts of the Yangtze block have different crustal structures, likely reflecting that they experienced different geological evolutionary processes. The spatial changes in structure and physical parameters of the northern block reflect the feature of “one cover and multiple bases” on the northern margin of the Yangtze block (Chang et al., 1991). The thin crust, high velocity, and high  $V_p/V_s$  ratios of the northern block were the result of geological processes such as Proterozoic accretion, Triassic collision, Mesozoic intracontinental orogeny, and Cretaceous crustal extension on the northern margin of the Yangtze block. The spatial changes in the structure and physical parameters of the southern block reflect the differences in the involvement of material of the southern margin of the Yangtze Craton into the Proterozoic collisional oro-

genic belt between the Yangtze and Cathaysian blocks, as shown by the development of relics of Proterozoic oceanic crust, arc volcanic rocks, and post-collision mafic rocks (<820 Ma) along the Jiangnan orogenic belt (Wang Y J et al., 2013). The thin crust, high velocity, and high  $V_p/V_s$  ratios of the southern block were the result of successive Proterozoic subduction, accretion and continental collision, Triassic collision with the Indosinian block, and Mesozoic intracontinental deformation (Zhang et al., 2012). In contrast, the central block retains well the basic characteristics of the Yangtze Craton, a relatively thick crust and relatively low S-wave velocity and  $V_p/V_s$  ratios, reflecting important events such as cratonization and Mesozoic intracontinental orogeny in this area.

## 5.2 Juvenile/ancient crustal formation and potential ore-forming sources

The inhomogeneities in the composition of the lower crust reflected by the regional variations in the velocity and  $V_p/V_s$  ratios of the lower crust of the Yangtze block can be further traced and constrained by zircon Hf-isotope mapping of crust-derived magmatic rocks because high  $\varepsilon_{\text{Hf}}(t)$  values reflect the contribution of new mantle-derived materials. The low  $\varepsilon_{\text{Hf}}(t)$  values indicate that the magma source included mainly ancient crustal materials, and the  $\varepsilon_{\text{Hf}}(t)$  value contour reflects the spatial distribution of different “crustal blocks” (Hou and Wang, 2018). Using samples of the Mesozoic magmatic rocks in the YMB, Yang et al. (2021) presented zircon Hf-isotope mapping results for the metallogenic belt and adjacent areas, which objectively reflect the spatial distribution and temporal evolutionary features of the crust with different properties. Based on this, we redrew the contour map of zircon Hf isotopes in combination with the new zircon Hf-isotope data of magmatic rocks exposed in the whole study area (Figure 12). These mapping results reveal the following important facts.

(1) The Hf isotopic composition of the Yangtze block displays obvious segmentation. In general, the southern block has a wide range of high  $\varepsilon_{\text{Hf}}(t)$  values, and the spatial distribution is consistent with the Jiangnan orogenic belt and the Dexing and other copper mineralization zones (Figure 12). The northern block has a low  $\varepsilon_{\text{Hf}}(t)$  background, and high values are observed within the main mineral deposits. The spatial distribution is consistent with the YMB, especially consistent with the locations of several ore-concentrated areas (e.g., Jurui, Anqing-Guichi, Ningwu, etc.) (Figure 12). The middle block shows transitional characteristics, dominated by relatively low  $\varepsilon_{\text{Hf}}(t)$  values; Zhuxi, Dahutang and other large and superlarge W deposits are areas with low  $\varepsilon_{\text{Hf}}(t)$  values (Figure 12). The spatial variation in the abovementioned Hf isotopic composition is generally in agreement with the variation trends of the P-wave velocity

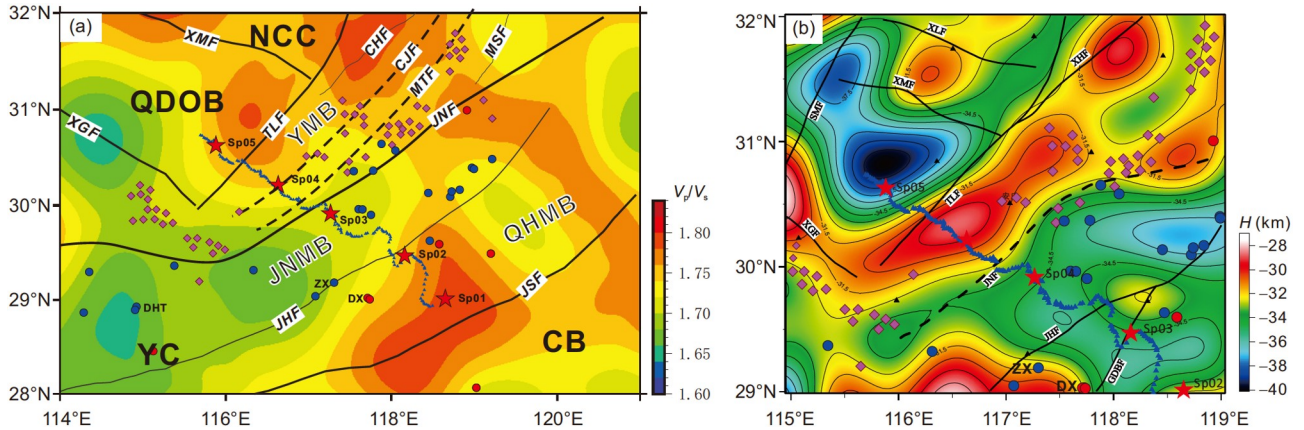


**Figure 11** (a)  $V_p/V_s$  ratio of the Yingshan-Changshan profile and adjacent areas, and (b) Moho depth.  $V_p/V_s$  ratio results modified from Zhang Y Q et al. (2021); and Moho depth derived from regional gravity (Yan et al., 2011).

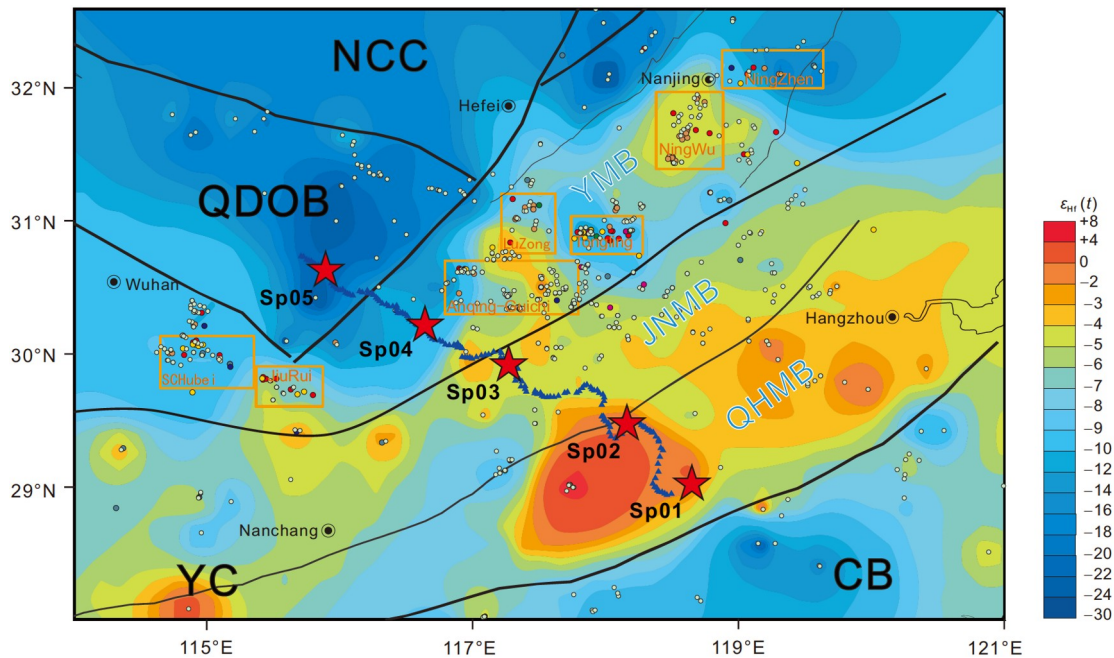


**Figure 12** Magmatic zircon Hf-isotope mapping results of the Yingshan-Changshan section and adjacent areas. This figure is redrawn based on Yang et al. (2021). The map mainly displays the Hf isotopic composition and its spatial variation in the Mesozoic magmatic crustal source area, reflecting the properties and spatial distribution of crustal blocks with different Hf values. The small circles in the figure represent sampling points, and the abbreviations are the same as in Figure 1.

and  $V_p/V_s$  value. This indicates that the areas with high  $\varepsilon_{\text{Hf}}(t)$  values are in line with the high velocity and high  $V_p/V_s$  regions and vice versa. These results indicate that the lower crust of the northern and southern margins of the Yangtze block is metamafic in composition and consists of more mantle-derived components, while the central part of the block is less mafic in composition and the amount of mantle-derived material is limited. The segmentation of  $\varepsilon_{\text{Hf}}(t)$  values, seismic velocity and  $V_p/V_s$  ratios and the difference in metal assemblages of the three metallogenic belts suggest that the crustal type and composition are genetically related to the spatial distribution and metal assemblage of the metallogenic belts (Lü et al., 2014, 2020; Yang et al., 2021).

(2) The crustal model age ( $T_{\text{DM}}^c$ ) can be calculated based on the zircon Hf-isotope composition, which can be used to reflect the age of the crustal material separated from the mantle source area and can be regarded as the formation time of the crust that is the source of the crust-derived magma (Hou et al., 2015; Hou and Wang, 2018). The  $T_{\text{DM}}^c$  mapping results of Yang et al. (2021) show that the spatial variations in the  $T_{\text{DM}}^c$  value and  $\varepsilon_{\text{Hf}}(t)$  value are generally negatively correlated. Among them, high  $T_{\text{DM}}^c$  values appear locally in the YMB and QHMB, while the central blocks show transitional features characterized by relatively high  $T_{\text{DM}}^c$  values (Yang et al., 2021). These results indicate that the Dabie orogenic belt and the North China Craton are dominated by

ancient crusts, while the Yangtze block crust may have undergone a reconstruction process (Ni and Wang, 2017), showing different degrees of juvenile material involvement. Within the Yangtze block, the lower crust of the northern and southern blocks may be dominated by juvenile crust, while the central block may be dominated by reworked crust.

The above arguments are strongly supported by several lines of evidence, mainly including the following. (1) Mesoproterozoic oceanic crust fragments (ophiolites), island arc basalts, and postcollision mafic rocks (Zhou and Li, 2000; Li et al., 2009; Zhang and Zheng, 2013) have been found in the northeastern segment of the Jiangnan Orogen and can be regarded as important juvenile mantle-derived mafic materials; they were injected into the bottom or interior of the ancient crust and were retained in the Neoproterozoic collisional orogenic belt. (2) The granite belt with high  $\varepsilon_{\text{Nd}}(t)$  values and low  $T_{\text{DM}}^c$  values developed along the JSF and its vicinity (Gilder et al., 1996; Hong et al., 2002), which is not only a material manifestation of the Neoproterozoic amalgamation of Yangtze and Cathaysia but also a magmatic record of the juvenile lower mafic crust that suffered from partial melting at a later stage. (3) Adakitic intrusive rocks widely exposed in the YMB are products of the partial melting of intermediate-mafic granulite in the lower crust (Zhang et al., 2001). The geochemistry of these adakitic rocks reflects the material composition of the lower crustal source. These Mesozoic adakitic rocks are characterized by wide variations in the initial values of  $\text{Sr}^{87}/\text{Sr}^{86}$ ,  $\varepsilon_{\text{Nd}}(t)$  and  $T_{\text{DM}}^c$ , indicating that the lower crust in this area may have suffered from underplating of young mantle-derived basaltic magmas (Zhang et al., 2001).

In fact, the extent of the juvenile lower crust in the YMB may be much larger than that revealed by Hf-isotope mapping. First, in some ore-concentrated areas (Ningwu, Luzong, etc.), some intermediate-mafic rock samples related to iron mineralization are included in isotopic mapping, and these rocks were mainly from the underlying enriched mantle (Yan et al., 2003). These rocks have a relatively negative  $\varepsilon_{\text{Hf}}(t)$  value due to metasomatism and enrichment (Griffin et al., 2013). Second, in some ore-concentrated areas, the Mesozoic magmatic assemblage is complex, and the composition varies greatly with xenolith inclusions inside the magmas, indicating that mantle-derived basaltic magmas not only underplate at the bottom of the crust but also have a high degree of magmatic mixing with crustal melts (Du et al., 2007; Meng et al., 2011), resulting in decreasing  $\varepsilon_{\text{Hf}}(t)$  values but also increasing  $T_{\text{DM}}^c$  values.

The genetic link between different crustal types and ore-bearing magmas, as well as their metal assemblages, has been confirmed by several studies. For example, the magma source of the Dexing porphyry copper deposit is considered to be a copper-rich juvenile lower crust involving mantle-

derived material (Wang Q et al., 2004; Hou et al., 2007), and this may represent remnants of the Neoproterozoic oceanic crustal fragments and magma arc roots retained in the lower crust during the collisional orogenic period, or this could represent large-scale underplating of pre-Mesozoic, mantle-derived magma at the bottom of the crust (Hou et al., 2013; Ni and Wang, 2017). The copper-bearing porphyries in the metallogenic belt of the YMB are dominated by adakitic rocks, which are believed to be mainly derived from the delaminated and thickened lower crust or the Cu-rich, mantle-derived magma underplated at the base of the crust (Wang Q et al., 2004; Hou et al., 2013; Zhou et al., 2017). The granite and porphyry systems related to tungsten deposits such as Zhuxi and Dahutang are believed to have originated from the Proterozoic W-rich metamorphic basement containing basalt interlayers (Huang and Jiang, 2013; Pan et al., 2012).

In summary, the YMB and QHMB have generally the same characteristics, which include thin crusts, high velocity anomalies, high wave velocity ratios and high  $\varepsilon_{\text{Hf}}(t)$  values, indicating that their lower crust was affected by newly formed, mantle-derived components. They eventually evolved into a juvenile mafic lower crust rich in Cu and Au, providing a key provenance for Mesozoic metallogenic magma and Cu-Au mineralization. The central JNMB has a low-velocity anomaly, low  $V_p/V_s$  ratios and low  $\varepsilon_{\text{Hf}}(t)$  values, reflecting that the W-rich ancient basement provides a possible material source for large-scale W mineralization.

### 5.3 The deep driving mechanisms of large-scale Cu-Au-W mineralization

Various models have been proposed for the dynamic mechanisms of Mesozoic tectonic magmatism and large-scale mineralization in South China, but any model should reasonably explain the following important observations: (1) Large-scale Cu-Au-W mineralization in the Mesozoic and the metallogenic timing show a northward younging trend, and the metal assemblage correspondingly has a gradual succession from Cu-Au to W, returning to Cu-Au again. (2) The P-wave velocity in South China is high in the upper part (0–70 km) and the lower part (300–400 km) but is low in the middle part (70–200 km), forming a “sandwich”-like structure (Lü et al., 2020). The 3-D shape of the low-velocity anomaly shows basic features of “deep in the south and shallow in the north” and a general tendency to the southwest (Jiang et al., 2013, 2015; Li et al., 2018). (3) The receiver function results show that the lithosphere of the Yangtze block significantly thinned to 60–80 km and that the lithosphere in the YMB is the thinnest (50–70 km) (Shi et al., 2013; Ye et al., 2019; Lü et al., 2021). (4) Teleseismic tomographic imaging and magnetotelluric detection results show that part of the lithosphere in the YMB and Jiangnan

orogenic belt was delaminated (Zhang et al., 2019; Lü et al., 2020).

The above observations seem to be related to an important unified deep process; that is, the lithosphere is thickened due to the Mesozoic intracontinental orogeny that underwent large-scale delamination, and the space left by the delamination was occupied by the rapidly upwelling asthenosphere. The low-velocity bodies appearing in a depth range of 70–200 km likely represent asthenospheric upwelling bodies that migrated and flowed gradually from deep to shallow depths and from the south to the north (Jiang et al., 2013; Lü et al., 2020). The high-temperature and fluid-rich asthenospheric material upwelled along the discontinuities and further deconstructed the lithosphere. This process also caused partial melting of the lithosphere and injected heat and fluid into the lower crust, leading to partial melting of the crust (Griffin et al., 2013) (Figure 13).

The Jiang-Shao fault (JSF), which lies on the southern side of the Jiangnan orogenic belt and acts as a lithospheric-scale boundary fault between the Yangtze and Cathaysian blocks, most likely represents the prime channel for asthenospheric upwelling. However, due to the very deep position

of the asthenospheric upwelling in this area (Jiang et al., 2013), it was difficult for the lithospheric mantle to melt, while the newly formed lower crust enriched in copper and gold could be heated and melted to form a porphyry system, forming the Dexing Cu deposit (~170 Ma). Over time, the upwelling asthenospheric body migrated northward (Jiang et al., 2013) and successively heated the crust of the central and northern parts of the Yangtze block. The ancient middle and lower crust in the central part melted, forming granite and porphyry in the forms of granitic stocks and growths, accompanied by large-scale tungsten mineralization (150–135 and 130–125 Ma, respectively). The juvenile lower crust in the north was partially melted, producing adakitic magmas leading to Cu-Au mineralization in the YMB (~140 Ma). The asthenosphere upwelled further and induced melting of the overlying lithospheric mantle to form intermediate-mafic magmatism and Fe mineralization (~130 Ma) (Figure 13).

The above conceptual models (Figure 13) imply that the faults cutting through the Moho and major block boundary faults are mechanically weak zones and play a role as channels for transporting heat from deep part and trans-

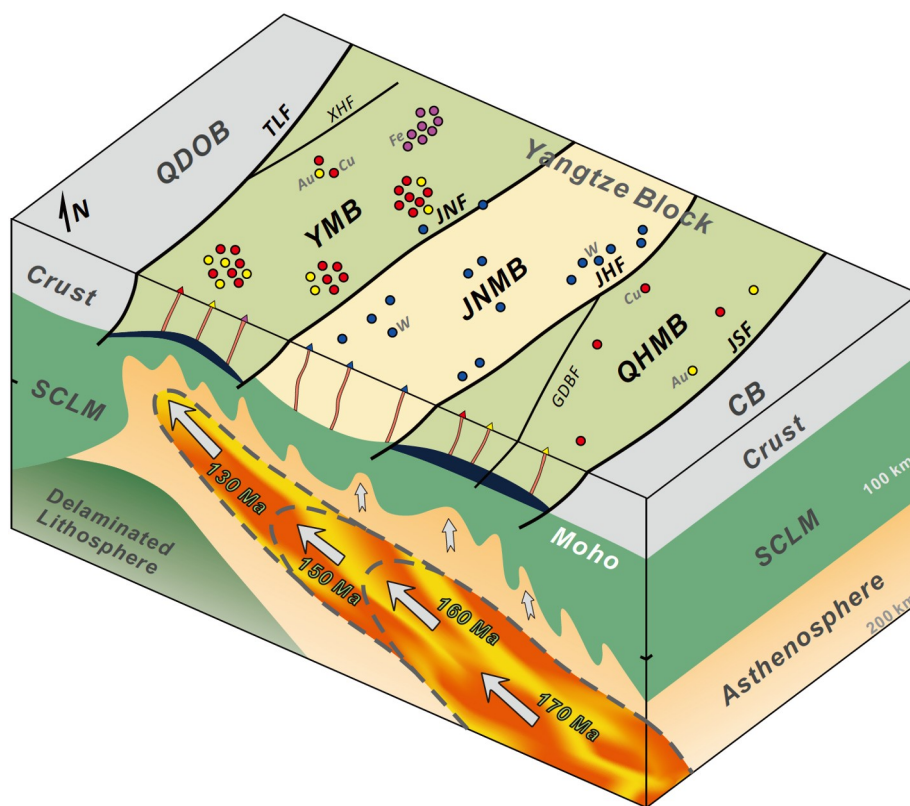


**Figure 13** Cartoon model showing the deep processes in northeastern South China and the control mechanisms on Mesozoic large-scale, Cu-Au-W mineralization. The main boundary faults and crustal structures in the figure are determined according to geological observations and geophysical survey data from this paper and previous studies (Lü et al., 2021), the thickness of the lithosphere is determined according to the research results of receiver functions (An and Shi, 2006; Lü et al., 2021), and the asthenosphere development location was determined based on tomographic results (Jiang et al., 2013). The delaminated lithosphere on the northern margin of the Yangtze block is inferred from the results of teleseismic tomography and magnetotelluric detection (Zhang et al., 2019; Lü et al., 2020). The dark blue bodies at the bottom of the crust in the YMB and QHMB represent the juvenile lower crust. Abbreviations in the figure are the same as those in Figure 1.

porting magmatic fluids upward and therefore undoubtedly played an important role in the mineralization process. Our velocity imaging clearly shows that the JNF in the YMB is a boundary fault dividing the crustal areas of its two sides (Figure 9), and the Moho beneath the buried Changjiang fault (CJF) and the main thrust fault (MTF), obviously uplifted, with the  $V_p/V_s$  ratios varying strikingly (Figure 11a). All of these faults played an important role in controlling regional mineralization. In the JNMB, the JNF and JHF, as important boundary faults (Figure 9), also worked similarly as channels for the transport of heat and magmatic fluids and therefore controlled the distribution of most large and super-large W deposits (Figure 1).

## 6. Conclusions

We construct the fine crustal structure based on a wide-angle, reflection/refraction seismic sounding profile between Yingshan and Changshan in eastern China. Based on the velocity model of our profile, we draw the following conclusions:

(1) The velocity structure of the Yingshan-Changshan profile is characterized by vertical layering and lateral segmentation. The velocity structure can be divided into three layers: the upper crust (~12 km), middle crust (~26 km), and lower crust (~31–35 km). Laterally, the crust can be divided into two high-velocity blocks located in the north and south and one low-velocity block located in the middle bounded by the Jiangnan fault and Jingdezhen-Huangshan fault in the north and south, respectively.

(2) In the northern block, the crust of the YMB has high velocity overall, the Moho interface was uplifted, the crust was thinned (~31 km), and the lower crust contains Cu-Au-rich mafic juvenile crust. The middle block (JNMB) generally shows low velocities at the crustal scale, and the lower crust is intermediate in composition with limited mantle-derived materials. The QHMB in the southern block shows high velocities, and its mafic juvenile lower crust is more likely to have formed during Proterozoic accretion/collision processes on the southern margin of the Yangtze block.

(3) Since the Mesozoic, the asthenospheric mantle has obliquely upwelled on a large scale from the Yangtze/Cathaysia collisional belt to the northern part of the Yangtze block and triggered partial melting of different types of crust. This was the deep driving mechanism of the explosive metallization of copper, gold and tungsten in the northeastern part of South China. Large-scale faults and block-boundary faults at the lithosphere scale form weak zones in the lithosphere, which were the main channels for transporting deep heat flow and magmatic fluids, thus controlling the regional distribution of metallogenic belts.

**Acknowledgements** We appreciate the Geophysical Exploration Center of China Earthquake Administration for providing seismic data. We are grateful to Baofeng LIU, Geophysical Exploration Center, China Earthquake Administration for valuable suggestions. We would thank Prof. Laicheng MIAO, Chenglong WU, Shi YAO and Xiangyang CHEN for their help. This work was supported by the National Key R&D Program of China (Grant Nos. 2019YFA0708602, 2019YFA0708603, and 2016YFC0600201), the National Natural Science Foundation of China (Grant Nos. 42130807, 42074099), and the China Geological Survey (Grant No. 1212011220243).

## References

- An M J, Shi Y L. 2006. Lithospheric thickness of the Chinese continent. *Phys Earth Planet Inter*, 159: 257–266
- Bai Z M, Wang C Y. 2006. Crustal P-wave velocity structure in Lower Yangtze region: Reinterpretation of Fulji-Fengxian deep seismic sounding profile. *Chin Sci Bull*, 51: 2391–2400
- Cerveny V, Klimes L, Psencik I. 1988. Complete seismic-ray tracing in three-dimensional structures. In: Doornbos D J, ed. *Seismological Algorithms*. New York: Academic Press. 89–168
- Cerveny V. 2001. *Seismic Ray Theory*. Cambridge: Cambridge University Press
- Chang Y F, Dong S W, Huang D Z. 1996. On the pattern and evolution of “one cover and multiple bottoms” in the middle-lower Yangtze (in Chinese). *Volcan Geol Miner*, 17: 1–15
- Chang Y F, Liu X P, Wu Y C. 1991. Copper-Iron Metallogenic Belt in the Middle and Lower Reaches of the Yangtze River (in Chinese). Beijing: Geological Press. 1–379
- Chang Y F, Zhou T F, Fan Y. 2012. Polygenetic compound mineralization and tectonic evolution: Study in the Middle-Lower Yangtze River Valley metallogenic belt (in Chinese). *Acta Petrol Sin*, 28: 3067–3075
- Chen G H, Shu L S, Shu L M, Zhang C, Ouyang Y P. 2016. Geological characteristics and mineralization setting of the Zhuxi tungsten (copper) polymetallic deposit in the Eastern Jiangnan Orogen. *Sci China Earth Sci*, 59: 803–823
- Chen H, Ni P, Chen R Y, Lü Z C, Ye T Z, Wang G G, Pan J Y, Pang Z S, Xue J L, Yuan H X. 2017. Constraints on the genesis of the Jiande polymetallic copper deposit in South China using fluid inclusion and O-H-Pb isotopes. *J Geol Soc India*, 90: 546–557
- Chen J F, Yan J, Xie Z, Xu X, Xing F. 2001. Nd and Sr isotopic compositions of igneous rocks from the Lower Yangtze region in eastern China: Constraints on sources. *Phys Chem Earth Part A-Solid Earth Geodesy*, 26: 719–731
- Dong S, Gao R, Cong B, Zhao Z, Liu X, Li S, Li Q, Huang D. 2004. Crustal structure of the southern Dabie ultrahigh-pressure orogen and Yangtze foreland from deep seismic reflection profiling. *Terra Nova*, 16: 319–324
- Dong S W, Ma L C, Liu G, Xue H M, Shi W, Li J H. 2011. On the metallogenic dynamics of the middle and lower reaches of the Yangtze River (in Chinese). *Acta Geol Sin*, 85: 612–625
- Dong S W, Wu X Z, Gao R, Lu D Y, Li Y K, He Y Q, Tong J F, Cao F Y, Hou M J, Huang D Z. 1998. Crustal velocity structure and dynamics of the Dabie orogenic belt (in Chinese). *Chin J Geophys*, 41: 349–361
- Dong S W, Xiang H S, Gao R, Lü Q T, Li J S, Zhan S Q, Lu Z W, Ma L C. 2010. Deep structure and ore formation within Lujiang-Zongyang volcanic ore concentrated area in Middle to Lower Reaches of Yangtze River (in Chinese). *Acta Petrol Sin*, 26: 2529–2542
- Dong S W, Zhang Y Q, Long C X, Yang Z Y, Ji Q, Wang T, Hu J M, Chen X H. 2007. New interpretation of Jurassic tectonic transformation and Yanshan movement in China (in Chinese). *Acta Geol Sin*, 81: 1449–1461
- Du Y S, Li S T, Cao Y, Qin X L, Lou Y E. 2007. Formation process of Mesozoic intrusive rocks in Tongguanshan mining area, Tongling, Anhui: Magma under-intrusion, assimilation and contamination and segregation crystallization (in Chinese). *Modern Geol*, 21: 71–77
- Duan D F, Jiang S Y. 2017. The composition of pyroxene and amphibole in

- ore-related pluton in Jiguanzui Au-Cu skarn deposit, Edong region: Implication for the magma evolution and mineralization (in Chinese). *Acta Petrol Sin*, 33: 3507–3517
- Duan Z, Liao S B, Chu P L, Huang W C, Zhu Y H, Shu X J, Li C B. 2019. Zircon U-Pb ages of the Neoproterozoic Jiuling complex granitoid in the eastern segment of the Jiangnan orogen and its tectonic significance (in Chinese). *Geol China*, 46: 493–516
- Feng C Y, Zhang D Q, Xiang X K, Li D X, Qu H Y, Liu J N, Xiao Y. 2012. Re-Os isotopic dating of molybdenite from the Dahutang tungsten deposit in northwestern Jiangxi Province and its geological implication (in Chinese). *Acta Petrol Sin*, 28: 3858–3868
- Gao S, Zhang B R, Jin Z M, Kern H, Luo T C, Zhao Z D. 1998. How mafic is the lower continental crust? *Earth Planet Sci Lett*, 161: 101–117
- Gilder S A, Gill J, Coe R S, Zhao X, Liu Z, Wang G, Yuan K, Liu W, Kuang G, Wu H. 1996. Isotopic and paleomagnetic constraints on the Mesozoic tectonic evolution of south China. *J Geophys Res*, 101: 16137–16154
- Gilder S A, Leloup P H, Courtillot V, Chen Y, Coe R S, Zhao X, Xiao W, Halim N, Cogné J P, Zhu R. 1999. Tectonic evolution of the Tancheng-Lujiang (Tan-Lu) fault via Middle Triassic to Early Cenozoic paleomagnetic data. *J Geophys Res*, 104: 15365–15390
- Griffin W L, Begg G C, O'Reilly S Y. 2013. Continental-root control on the genesis of magmatic ore deposits. *Nat Geosci*, 6: 905–910
- Gu Q P, Ding Z F, Kang Q Q, Li D H. 2020. Group velocity tomography of Rayleigh wave in the middle-southern segment of the Tan-Lu fault zone and adjacent regions using ambient seismic noise (in Chinese). *Chin J Geophys*, 63: 1505–1522
- He Z Y, Xu X S, Chen R, King G F. 2007. Genesis of Middle Jurassic syenite-gabbro in southern Jiangxi province and their geological significance (in Chinese). *Acta Petrol Sin*, 23: 1457–1469
- Hong D W, Xie X L, Zhang J S. 2002. Analysis of the geological significance of the Hangzhou-Zhuguangshan-Huashan high  $\epsilon_{\text{Nd}}$  granite belt (in Chinese). *Geol Bull*, 21: 348–354
- Hou Z Q, Duan L F, Lu Y J, Zheng Y C, Zhu D C, Yang Z M, Yang Z S, Wang B D, Pei Y R, Zhao Z D, McCuaig T C. 2015. Lithospheric architecture of the Lhasa Terrane and its control on ore deposits in the Himalayan-Tibetan Orogen. *Econ Geol*, 110: 1541–1575
- Hou Z Q, Pan X F, Yang Z M, Qu X M. 2007. A Preliminary Discussion on Porphyry Copper Deposits in Continental Environment (in Chinese). *Modern Geol*, 21: 332–351
- Hou Z Q, Wang T. 2018. Isotopic mapping and deep material probing(II): Imaging crustal architecture and its control on mineral systems (in Chinese). *Earth Sci Front*, 25: 20–41
- Hou Z Q, Yang Z S, Li Y Q, Zeng P S, Meng Y F, Xu W Y, Tian S H. 2004. Large-scale migration and convergence of fluids in the foreland basin during collisional orogeny: From Triassic gypsum-salt formation and regional alteration in the middle and lower reaches of the Yangtze River evidence (in Chinese). *Geol Miner Deposit*, 23: 310–327
- Hou Z, Pan X, Li Q, Yang Z, Song Y. 2013. The giant Dexing porphyry Cu-Mo-Au deposit in east China: Product of melting of juvenile lower crust in an intracontinental setting. *Miner Depos*, 48: 1019–1045
- Hsü K J, Li J L, Chen H H, Wang Q C, Sun S, Sengor A M C. 1990. Tectonics of South China: Key to understanding West Pacific geology. *Tectonophysics*, 183: 9–39
- Hsü K J, Shu S, Jiliang L, Haihong C, Haipo P, Sengor A M C. 1988. Mesozoic overthrust tectonics in south China. *Geology*, 16: 418–421
- Huang L C, Jiang S Y. 2013. Geochronology, geochemistry and petrogenesis of the tungsten-bearing porphyritic granite in the Dahutang tungsten deposit, Jiangxi Province (in Chinese). *Acta Petrol Sin*, 29: 4323–4335
- Ji S C, Wang Q, Salisbury M H. 2009. Composition and tectonic evolution of the Chinese continental crust constrained by Poisson's ratio. *Tectonophysics*, 463: 15–30
- Jiang G M, Zhang G B, Lü Q T, Shi D N, Xu Y. 2013. 3-D velocity model beneath the Middle-Lower Yangtze River and its implication to the deep geodynamics. *Tectonophysics*, 606: 36–47
- Jiang G M, Zhang G B, Zhao D P, Lu Q T, Li H Y, Li X F. 2015. Mantle dynamics and Cretaceous magmatism in east-central China: Insight from teleseismic tomograms. *Tectonophysics*, 664: 256–268
- Jiang G M, Zhang G B, Lü Q T, Shi D N, Xu Y. 2014. Deep geodynamics of mineralization beneath the Middle-Lower Reaches of Yangtze River: Evidence from teleseismic tomography (in Chinese). *Acta Petrol Sin*, 30: 907–917
- Li H Y, Song X D, Lü Q T, Yang X Y, Deng Y F, Ouyang L B, Li J P, Li X F, Jiang G M. 2018. Seismic imaging of lithosphere structure and upper mantle deformation beneath east-central China and their tectonic implications. *J Geophys Res-Solid Earth*, 123: 2856–2870
- Li T Z, Zhao L, Wan B, Li Z W, Bodin T, Wang K, Yuan H Y. 2020. New crustal  $V_s$  model along an array in south-east China: Seismic characters and Paleo-Tethys continental amalgamation. *Geochem Geophys Geosyst*, 21: e09024
- Li X H, Li W X, Li Z X, Lo C H, Wang J, Ye M F, Yang Y H. 2009. Amalgamation between the Yangtze and Cathaysia Blocks in South China: Constraints from SHRIMP U-Pb zircon ages, geochemistry and Nd-Hf isotopes of the Shuangxiwu volcanic rocks. *Precambrian Res*, 174: 117–128
- Li X H, Li Z X, Li W X, Wang Y. 2006. Initiation of the Indosinian Orogeny in South China: Evidence for a Permian magmatic arc on Hainan Island. *J Geol*, 114: 341–353
- Li X H, Zhao J X, McCulloch M T, Zhou G Q, Xing F M. 1997. Geochemical and Sm-Nd isotopic study of Neoproterozoic ophiolites from southeastern China: Petrogenesis and tectonic implications. *Precambrian Res*, 81: 129–144
- Li Z X, Li X H. 2007. Formation of the 1300-km-wide intracontinental orogen and postorogenic magmatic province in Mesozoic South China: A flat-slab subduction model. *Geology*, 35: 179
- Liu F T, Xu P F, Liu J S, Yin Z X, Qin J Y, Zhang X K, Zhang C K, Zhao J R. 2003. Crustal velocity structure of continental deep subduction zone—A Study of deep earthquake wide-angle reflection/refraction in East Dabie Orogen (in Chinese). *Chin J Geophys*, 46: 366–372
- Liu Q Y, He L J, Huang F. 2013. Review of Mesozoic geodynamics research of South China (in Chinese). *Prog Geophys*, 28: 633–647
- Lü Q T, Dong S W, Shi D N, Tang J T, Jiang G M, Zhang Y Q, Xu T, SinoProbe-03-CJ Group. 2014. Lithosphere architecture and geodynamic model of Middle and Lower Reaches of Yangtze Metallogenic Belt: A review from SinoProbe (in Chinese). *Acta Petrol Sin*, 30: 889–906
- Lü Q T, Dong S W, Tang J T, Shi D N, Chang Y F, SinoProbe-03-CJ Group. 2015a. Multi-scale and integrated geophysical data revealing mineral systems and exploring for mineral deposits at depth: A synthesis from SinoProbe-03 (in Chinese). *Chin J Geophys*, 58: 4319–4343
- Lü Q T, Shi D N, Liu Z D, Zhang Y Q, Dong S W, Zhao J H. 2015b. Crustal structure and geodynamics of the Middle and Lower reaches of Yangtze metallogenic belt and neighboring areas: Insights from deep seismic reflection profiling. *J Asian Earth Sci*, 114: 704–716
- Lü Q T, Hou Z Q, Yang Z S, Shi D N. 2005. Underplating in the middle-lower Yangtze Valley and model of geodynamic evolution: Constraints from geophysical data. *Sci China Ser D-Earth Sci*, 48: 985–999
- Lü Q T, Hou Z Q, Zhao J H, Shi D N, Wu X Z, Chang Y F, Pei R F, Huang D D, Kuang C Y. 2004. Deep seismic reflection profiling revealing the complex crustal structure of the Tongling ore district. *Sci China Ser D-Earth Sci*, 47: 193–200
- Lü Q T, Meng G X, Yan J, Zhang K, Gong X J, Gao F X. 2020. The geophysical exploration of Mesozoic iron-copper mineral system in the Middle and Lower Reaches of the Yangtze River Metallogenic Belt: A synthesis (in Chinese). *Earth Sci Front*, 27: 232–253
- Lü Q T, Meng G X, Zhang K, Liu Z D, Yan J Y, Shi D N, Han J G, Gong X J. 2021. The lithospheric architecture of the Lower Yangtze Metallogenic Belt, East China: Insights into an extensive Fe-Cu mineral system. *Ore Geol Rev*, 132: 103989
- Lü Q T, Shi D N, Tang J T, Wu M G, Chang Y F, SinoProbe-03-CJ project Group. 2011. Deep structural exploration of metallogenic belts and typical ore concentration areas in the middle and lower reaches of the Yangtze River (in Chinese). *Acta Geosci Sin*, 32: 257–268
- Lü Q T, Yan J Y, Shi D N, Dong S W, Tang J T, Wu M G, Chang Y F.

2013. Reflection seismic imaging of the Lujiang-Zongyang volcanic basin, Yangtze Metallogenic Belt: An insight into the crustal structure and geodynamics of an ore district. *Tectonophysics*, 606: 60–77
- Lü Q T, Yang Z S, Yan J Y, Xu W Y. 2007. The metallogenic potential, prospecting ideas and preliminary attempts of the deep metallogenic belt in the middle and lower reaches of the Yangtze River—Taking the Tongling ore cluster as an example (in Chinese). *Chin J Geology*, 81: 865–881
- Luo S, Yao H, Li Q, Wang W, Wan K, Meng Y, Liu B. 2019. High-resolution 3D crustal S-wave velocity structure of the Middle-Lower Yangtze River Metallogenic Belt and implications for its deep geodynamic setting. *Sci China Earth Sci*, 62: 1361–1378
- Luo Y H, Xu Y X, Yang Y J. 2012. Crustal structure beneath the Dabie orogenic belt from ambient noise tomography. *Earth Planet Sci Lett*, 313-314: 12–22
- Mao J W, Wang Y T, Lehmann B, Yu J J, Du A D, Mei Y X, Li Y F, Zang W S, Stein H J, Zhou T F. 2006. Molybdenite Re-Os and albite  $^{40}\text{Ar}/^{39}\text{Ar}$  dating of Cu-Au-Mo and magnetite porphyry systems in the Yangtze River valley and metallogenic implications. *Ore Geol Rev*, 29: 307–324
- Mao J W, Wu S H, Song S W, D P, Xie G Q, Su Q W, Liu P, Wang X G, Yu Z Z, Chen X X, Tang W X. 2020. The world-class Jiangnan tungsten belt: Geological characteristics, metallogeny, and ore deposit model (in Chinese). *Chin Sci Bull*, 65: 3746–3762
- Meng X J, Lü Q T, Yang Z S, Xu W Y. 2011. Geochemical characteristics of Mesozoic intermediate-acid intrusive rocks in Tongling and adjacent areas in the middle and lower reaches of the Yangtze River and their deep magmatism (in Chinese). *Acta Geol Sin*, 85: 757–777
- Ni P, Wang G G. 2017. Multiple episodes of Cu-Au mineralization in the northeastern section of the Qin-Hang metallogenic belt induced by reworking of continental crust (in Chinese). *Acta Petrol Sin*, 33: 3373–3394
- Ouyang L B, Li H Y, Lü Q T, Yang Y J, Li X F, Jiang G M, Zhang G B, Shi D N, Zheng D, Sun S J, Tan J, Zhou M. 2014. Crustal and uppermost mantle velocity structure and its relationship with the formation of ore districts in the Middle-Lower Yangtze River region. *Earth Planet Sci Lett*, 408: 378–389
- Ouyang Y P, Rao J F, Liao S P, He X R, Hu Q H, Wei J, Yang M G. 2019. Rock- and ore-controlling structure in the Zhuxi ore concentration area in the northeastern Jiangxi Province (in Chinese). *Geol China*, 46: 878–893
- Pan X F, Song Y C, Li Z Q, Hu B G, Zhu X Y, Wang Z K, Yang D, Zhang T F, Li Y. 2012. Alteration-mineralization system fluid evolution of the Dexing Tongchang porphyry copper (molybdenum-gold) deposit: H-O isotopic constraints (in Chinese). *Deposit Geol*, 31: 850–860
- Pan Y M, Dong P. 1999. The Lower Changjiang (Yangzi/Yangtze River) metallogenic belt, east central China: Intrusion- and wall rock-hosted Cu-Fe-Au, Mo, Zn, Pb, Ag deposits. *Ore Geol Rev*, 15: 177–242
- Richards J P. 2011. Magmatic to hydrothermal metal fluxes in convergent and collided margins. *Ore Geol Rev*, 40: 1–26
- Shi D N, Lü Q T, Xu W Y, Yan J Y, Zhao J H, Dong S W, Chang Y F, SinProbe-03-02 team. 2013. Crustal structure beneath the middle-lower Yangtze metallogenic belt in East China: Constraints from passive source seismic experiment on the Mesozoic intra-continental mineralization. *Tectonophysics*, 606: 48–59
- Song C Z, Zhang H, Ren S L, Li J H, Tu W C, Zhang Y, Wang Z. 2011. Analysis of the transformation structure and regional metallogenic background in the middle and lower reaches of the Yangtze River (in Chinese). *Chin J Geology*, 85: 778–788
- Sun W, Ding X, Hu Y H, Li X H. 2007. The golden transformation of the Cretaceous plate subduction in the west Pacific. *Earth Planet Sci Lett*, 262: 533–542
- Sun W D, Xie Z, Chen J F, Zhang X, Chai Z F, Du A D, Zhao J S, Zhang C H, Zhou T F. 2003. Os-Os dating of copper and molybdenum deposits along the middle and lower reaches of the Yangtze River, China. *Econ Geol*, 98: 175–180
- Vidale J E. 1988. Finite-difference calculation of travel times. *Bull Seismol Soc Am*, 78: 2062–2076
- Wang C Y, Zeng R S, Mooney W D, Hacker B R. 2000. A crustal model of the ultrahigh-pressure Dabie Shan orogenic belt, China, derived from deep seismic refraction profiling. *J Geophys Res*, 105: 10857–10869
- Wang D, Wang X L, Cai Y, Chen X, Zhang F R, Zhang F F. 2017. Heterogeneous conservation of zircon xenocrysts in Late Jurassic granitic intrusions within the Neoproterozoic Jiuling Batholith, South China: A magma chamber growth model in deep crustal hot zones. *J Petrol*, 58: 1781–1810
- Wang F Y, Ling M X, Ding X, Hu Y H, Zhou J B, Yang X Y, Liang H Y, Fan W M, Sun W. 2011. Mesozoic large magmatic events and mineralization in SE China: Oblique subduction of the Pacific plate. *Int Geol Rev*, 53: 704–726
- Wang G G, Ni P, Wang R C, Zhao K D, Chen H, Ding J Y, Zhao C, Cai Y T. 2013. Geological, fluid inclusion and isotopic studies of the Yinshan Cu-Au-Pb-Zn-Ag deposit, South China: Implications for ore genesis and exploration. *J Asian Earth Sci*, 74: 343–360
- Wang G G, Ni P, Yao J, Wang X L, Zhao K D, Zhu R Z, Xu Y F, Pan J Y, Li L, Zhang Y H. 2015. The link between subduction-modified lithosphere and the giant Dexing porphyry copper deposit, South China: Constraints from high-Mg adakitic rocks. *Ore Geol Rev*, 67: 109–126
- Wang Q C. 2009. A brief discussion on the sedimentary tectonic problems of the South China continental block group (in Chinese). *Acta Sedimentol Sin*, 27: 811–817
- Wang Q, Xu J F, Zhao Z H, Bao Z W, Xu W, Xiong X L. 2004. Cretaceous high-potassium intrusive rocks in the Yueshan-Hongzhen area of east China: Adakites in an extensional tectonic regime within a continent. *Geochem J*, 38: 417–434
- Wang Q. 2007. Experimental and theoretical study on the properties of seismic waves in rocks (in Chinese). *Bull Mineral Petrol Geochem*, 26: 118–126
- Wang X L, Liu J X, Lü Q T, Wang S, Wang D, Chen X. 2021. Evolution of deep crustal hot zones constrained by the diversity of Late Mesozoic magmatic rocks in SE China. *Ore Geol Rev*, 134: 104143
- Wang X L, Zhou J C, Chen X, Zhang F F, Sun Z M. 2017. Formation and evolution of the Jiangnan orogenic belt (in Chinese). *Bull Mineral Petrol Geochem*, 36: 714–735
- Wang Y J, Zhang A M, Cawood P A, Fan W M, Xu J F, Zhang G W, Zhang Y Z. 2013. Geochronological, geochemical and Nd-Hf-Os isotopic fingerprinting of an early Neoproterozoic arc-back-arc system in South China and its accretionary assembly along the margin of Rodinia. *Precambrian Res*, 231: 343–371
- Wang Y, Deng J F, Ji G Y. 2004. A perspective on the geotectonic setting of early Cretaceous adakite-like rocks in the Lower Reaches of Yangtze River and its significance for Cu-Au mineralization (in Chinese). *Acta Petrologica Sinica*, 20: 297–314
- Xiang X K, Liu X M, Zhan G N. 2012. Discovery and prospecting significance of super-large tungsten deposits in Shimensi mining area, Dahutang, Jiangxi Province (in Chinese). *Resour Invest Environ*, 33: 142–151
- Xie D K, Mao J R, Peng W Z, Zhao Y, Jiang Y H. 1997. Lithostratigraphy and continental dynamics in South China (in Chinese). *Chin J Geophys*, S1: 153–163
- Xing F M, Xu X. 1999. The Yangtze Magmatic Belt and Mineralization in Anhui (in Chinese). Hefei: Anhui People's Publishing House
- Xu J, Zhu G, Tong W, Cui K, Liu Q. 1987. Formation and evolution of the Tancheng-Lujiang wrench fault system: A major shear system to the northwest of the Pacific Ocean. *Tectonophysics*, 134: 273–310
- Xu T, Li F, Wu Z B, Wu C L, Gao E G, Zhou B, Zhang Z J, Xu G M. 2014a. A successive three-point perturbation method for fast ray tracing in complex 2D and 3D geological models. *Tectonophysics*, 627: 72–81
- Xu T, Xu G M, Gao E G, Li Y C, Jiang X Y, Luo K. 2006a. Block modeling and segmentally iterative ray tracing in complex 3D media. *Geophysics*, 71: T41–T51
- Xu T, Xu G M, Gao E G, Zhu L B, Jiang X Y. 2004. Block modeling and shooting ray tracing in complex 3-D media (in Chinese). *Chin J Geophys*, 47: 1118–1126

- Xu T, Zhang Z J, Gao E G, Xu G M, Sun L. 2010. Segmentally iterative ray tracing in complex 2D and 3D heterogeneous block models. *Bull Seismol Soc Am*, 100: 841–850
- Xu T, Zhang Z J, Tian X B, Liu B F, Bai Z M, Lü Q T, Teng J W. 2014b. Crustal structure beneath the Middle-Lower Yangtze metallogenic belt and its surrounding areas: Constraints from active source seismic experiment along the Lixin to Yixing profile in East China (in Chinese). *Acta Petrol Sin*, 30: 918–930
- Xu Z Q, Wang Q, Ji S C, Chen J, Zeng L S, Yang J S, Chen F Y, Liang F H, Wenk H R. 2006b. Petrofabrics and seismic properties of garnet peridotite from the UHP Sulu terrane (China): Implications for olivine deformation mechanism in a cold and dry subducting continental slab. *Tectonophysics*, 421: 111–127
- Yan J Y, Lü Q T, Meng G X, Zhao J H, Deng Z, Liu Y. 2011. Study on the structural framework of the metallogenic belt in the middle and lower reaches of the Yangtze River based on gravity and magnetic multi-scale edge detection (in Chinese). *Chin J Geology*, 85: 900–914
- Yan J, Chen J F, Yu G, Qian H, Zhou C X. 2003. Lead isotope characteristics of late Mesozoic mesobasic rocks in the middle and lower reaches of the Yangtze River: Evidence of enrichment in the mantle (in Chinese). *J Geol Univ*, 9: 196–205
- Yang D, Lü Q T, Yang Z S, Yan J Y, Xiong X, Chen Y X. 2021. Zircon Hf-isotopic mapping of Middle-Lower Yangtze River Valley Metallogenic Belt, China: Constraints on crustal properties and ore cluster formation. *Lithos*, 406-407: 106526
- Yang M G, Mei Y W. 1997. Main features of the Qin-Hanggu plate junction and metallogenic belts (in Chinese). *South China Geol Miner*, (3): 52–59
- Yao J L, Cawood P A, Shu L S, Santosh M, Li J Y. 2016. An Early Neoproterozoic accretionary prism ophiolitic melange from the western Jiangnan Orogenic Belt, South China. *J Geol*, 124: 587–601
- Ye Z, Li Q S, Zhang H S, L J G, Wang X R, Han R B, Wu Q J. 2019. Crustal and uppermost mantle structure across the Lower Yangtze region and its implications for the late Mesozoic magmatism and metallogenesis, eastern South China. *Phys Earth Planet Inter*, 297: 106324
- Zandt G, Ammon C J. 1995. Continental crust composition constrained by measurements of crustal Poisson's ratio. *Nature*, 374: 152–154
- Zelt C A, Smith R B. 1992. Seismic traveltimes inversion for 2-D crustal velocity structure. *Geophys J Int*, 108: 16–34
- Zhai Y S, Yao S Z, Lin X D, Jin F Q, Zhou X R, Wan T F, Zhou Z G. 1992. Study on the metallogenic regularity of iron and copper in the middle and lower reaches of the Yangtze River (in Chinese). *Geol Miner Deposit*, 11: 1–12
- Zhang K, Lü Q T, Yan J Y, Hu H, Fu G M, Luo F. 2019. The three-dimensional electrical structure and metallogenic prospect of the Ning (Nanjing)-Wu (Wuhu) basin and the southern adjacent area in eastern China. *J Asian Earth Sci*, 173: 304–313
- Zhang M H, Xu T, Lü Q T, Bai Z M, Wu C L, Wu Z B, Teng J W. 2015. 3D Moho depth beneath the middle-lower Yangtze metallogenic belt and its surrounding areas: Insight from the wide angle seismic data (in Chinese). *Chin J Geophys*, 58: 4360–4372
- Zhang Q, Jin Wei J, Li C D, Wang Y L. 2009. Yamhanian large-scale magmatism and lithosphere thinning in Eastern China: Relation to large igneous province (in Chinese). *Earth Sci Front*, 16: 21–51
- Zhang Q, Wang Y, Qian Q, Yang J H, Wang Y L, Zhao T P, Guo G J. 2001. The characteristics and tectonic-metallogenic significances of the adakites in Yanshan period from eastern China (in Chinese). *Acta Petrol Sin*, 17: 236–244
- Zhang Y Q, Dong S W, Li J H, Cui J J, Shi W, Su J B, Li Y. 2012. New progress in Mesozoic tectonic research in South China (in Chinese). *Acta Geosci Sin*, 33: 257–279
- Zhang Y Q, Lü Q T, Teng J W, Wang Q S, Xu T. 2014. Discussion on the crustal density structure and deep mineralization background in the Middle-Lower Yangtze metallogenic belt and its surrounding areas: Constraints from the gravity inversion (in Chinese). *Acta Petrol Sin*, 30: 931–940
- Zhang Y Q, Shi D N, Lü Q T, Xu Y, Xu Z W, Yan J Y, Chen C X, Xu T. 2021. The crustal thickness and composition in the eastern South China Block constrained by receiver functions: Implications for the geological setting and metallogenesis. *Ore Geol Rev*, 130: 103988
- Zhang Z J, Chen Q F, Bai Z M, Chen Y, Badal J. 2011a. Crustal structure and extensional deformation of thinned lithosphere in Northern China. *Tectonophysics*, 508: 62–72
- Zhang Z J, Yang L Q, Teng J W, Badal J. 2011b. An overview of the earth crust under China. *Earth-Sci Rev*, 104: 143–166
- Zhang Z, Deng Y F, Yao J M, Zong J Y, Chen H Y. 2021. An array based seismic image on the Dahutang deposit, South China: Insight into the mineralization. *Phys Earth Planet Inter*, 310: 106617
- Zhang S B, Zheng Y F. 2013. Formation and evolution of Precambrian continental lithosphere in South China. *Gondwana Res*, 23: 1241–1260
- Zhao G C. 2015. Jiangnan orogen in South China: Developing from divergent double subduction. *Gondwana Res*, 27: 1173–1180
- Zheng T Y, Zhao L, He Y M, Zhu R X. 2014. Seismic imaging of crustal reworking and lithospheric modification in eastern China. *Geophys J Int*, 196: 656–670
- Zheng Y F, Wu R X, Wu Y B, Zhang S B, Yuan H, Wu F Y. 2008. Rift melting of juvenile arc-derived crust: Geochemical evidence from Neoproterozoic volcanic and granitic rocks in the Jiangnan Orogen, South China. *Precambrian Res*, 163: 351–383
- Zhou T F, Fan Y, Wang S W and White N C. 2017. Metallogenic regularity and metallogenic model of the Middle-Lower Yangtze River Valley Metallogenic Belt (in Chinese). *Acta Petrol Sin*, 33: 3353–3372
- Zhou T F, Fan Y, Yuan F, Lu S M, Shang S G, Cooke D, Meffre S, Zhao G C. 2008a. Geochronology of the volcanic rocks in the Lu-Zong basin and its significance. *Sci China Ser D-Earth Sci*, 51: 1470–1482
- Zhou T F, Fan Y, Yuan F. 2008b. Advances on petrogenesis and metallogeny study of the mineralization belt of the Middle and Lower Reaches of the Yangtze River area (in Chinese). *Acta Petrol Sin*, 24: 1665–1678
- Zhou X M, Li W X. 2000. Origin of Late Mesozoic igneous rocks in Southeastern China: Implications for lithosphere subduction and underplating of mafic magmas. *Tectonophysics*, 326: 269–287
- Zhu G, Wang D X, Liu G S, Niu M L, Song C Z. 2004a. Evolution of the Tanlu fault zone and its response to the motion of the western Pacific plate (in Chinese). *Geol Sci*, 39: 36–49
- Zhu G, Wang Y S, Liu G S, Niu M L X C L, Li C C. 2005.  $^{40}\text{Ar}/^{39}\text{Ar}$  dating of strike-slip motion on the Tan-Lu fault zone, East China. *J Struct Geol*, 27: 1379–1398
- Zhu G, Wang Y S, Niu M L, Liu G S, Xie C L. 2004b. Co-orogenic movement of the Tanlu fault zone (in Chinese). *Earth Sci Front*, 11: 169–182

(Responsible editor: Dinghui YANG)